Available online at www.sciencedirect.com
ScienceDirect
Journal of Electroanalytical Chemistry 601 (2007) 194–204
Journal of Electroanalytical Chemistry
www.elsevier.com/locate/jelechem

Comparative cyclic voltammetry and SEM analysis of tin electrodes in citrate buffer solutions

C.A. Gervasi [a,b,*], P.E. Alvarez [c], M.V. Fiori Bimbi [c], M.E. Folquer [d]

[a] Instituto de Investigaciones Fisicoquímicas Teóricas y Aplicadas (INIFTA), Facultad de Ciencias Exactas, Universidad Nacional de La Plata, Sucursal 4-C.C. 16, 1900 La Plata, Argentina
[b] Laboratorio de Ingeniería de Corrosión y Tecnología Electroquímica (LICTE), Facultad de Ingeniería, Universidad Nacional de La Plata, 1 y 47, 1900 La Plata, Argentina
[c] Instituto de Física, Facultad de Bioquímica, Química y Farmacia, Universidad Nacional de Tucumán, Ayacucho 491, 4000 Tucumán, Argentina
[d] Instituto de Química Física, Facultad de Bioquímica, Química y Farmacia, Universidad Nacional de Tucumán, Ayacucho 491, 4000 Tucumán, Argentina

Received 14 August 2006; received in revised form 31 October 2006; accepted 16 November 2006
Available online 22 December 2006

Abstract

The anodic oxidation of tin in citrate buffer solutions has been studied by cyclic voltammetry and scanning electron microscopy. In order to identify each individual process, a numerical method was used to resolve into single processes the electrochemical behaviour. The results indicate that primary passivation is due to the formation of a Sn(II)-containing surface film. This film is not further oxidized at higher anodic potentials. There is evidence that during secondary passivation direct oxidation of Sn to Sn(IV) takes place, either as soluble ions or as a hydroxide layer. The results of this work improve, as well as, confirm theories previously advanced.

Keywords: Tin; Citrate buffer; Passive films; Voltammetry; SEM

1. Introduction

Much attention was devoted to the electrochemical behaviour of tin due to its widespread technological applications. Studies of the anodic passivation of tin electrodes in carboxylic acids and the so-called fruit acids are relevant, in particular, to the manufacture of tinplate and its use in the food industry [1,2].

Voltammetric studies used to elucidate the electrooxidation of tin in solutions of citric acid were interpreted as the formation of Sn(II) species that are oxidized to Sn(IV), while passive film formation results from hydrolysis of Sn(IV) species with subsequent dehydration [3]. There is general agreement that corrosion resistance of tin results from a thin surface oxide layer of SnO_2 [4]. Šeruga and Metikoš-Huković [5,6] showed that properties of the film electrogenerated in citrate buffer solutions depend significantly on the pH value and that tin–citric acid complexes could participate in the film formation.

In order to further clarify the disagreement in the literature concerning the composition of the passive film on tin and the mechanism of its formation, Keller and Strehblow developed a model of the passive layer. This model is based on results of XPS studies on tin in KOH [7], but similar results were obtained in a buffer solution at pH 5.5 [8]. The films obtained potentiostatically in the passive potential range were interpreted as consisting mainly of SnO_2 with a small contribution of SnO. Tin hydroxide was found only on top of the layer, while SnO was detected underneath a layer of SnO_2 having a constant thickness irrespective of the formation potential.

* Corresponding author. Address: Instituto de Investigaciones Fisicoquímicas Teóricas y Aplicadas (INIFTA), Facultad de Ciencias Exactas, Universidad Nacional de La Plata, Sucursal 4-C.C. 16, 1900 La Plata, Argentina. Tel.: +54 221 425 7430; fax: +54 221 425 4642.
E-mail address: gervasi@inifta.unlp.edu.ar (C.A. Gervasi).

0022-0728/$ - see front matter © 2006 Elsevier B.V. All rights reserved.
doi:10.1016/j.jelechem.2006.11.019

However, the fact that the full picture of the potentiodynamic response of tin electrodes in citrate buffer solutions has not yet been established, was our motivation to revisit this issue.

2. Experimental

The experimental arrangement was described in previous publications [9]. "Specpure" tin in the form of both static and rotating discs (Johnson Matthey Chemical Ltd., 0.30 cm^2 apparent area) axially mounted in PTFE holders were used as working electrodes. The exposed tin surface was mechanically ground down to a mirror finish with 1.0 and 0.3 μm alumina powder, rinsed in triply distilled water and held for a time $\tau_o = 15$ min at potentials sufficiently negative to produce a net hydrogen evolution. The counter-electrode was a large area Pt sheet. Potentials were measured and referred to in the text against a saturated calomel electrode (sce) (0.242 V in the nhe scale).

Experiments were made under purified N_2 gas saturation at 25 °C. Potentiodynamic experiments were performed in solutions containing x M sodium citrate dihydrate + y M anhydrous citric acid, with x and y varied conveniently to cover the 3–6 pH range (at constant ionic strength $I = 0.1167$), and to cover the 0.1–1.2 ionic strength (I) range (at constant pH = 5). Electrolytes were prepared from analytical grade (p.a. Merck) chemicals and triply distilled water.

Voltammograms were recorded for electrodes either still ($\omega = 0$) or under rotation ($500 \leqslant \omega \leqslant 2500$ rpm) by employing the following perturbating potential programmes: single and repetitive triangular potential sweeps (STPS and RTPS, respectively) between preset cathodic ($E_{s,c}$) and anodic ($E_{s,a}$) switching potentials at potential scan rates (v) in the 0.0015 V $s^{-1} \leqslant v \leqslant 0.3$ V s^{-1} range.

Impedance spectra were recorded for each solution using a Solartron SI 1254 device; a 10 mV amplitude sine-wave signal perturbation was applied in the high frequency range in order to measure the uncompensated electrolyte resistance [10]. Accordingly, voltammograms were corrected by ohmic drop.

Scanning electron microscopy (SEM) examination was performed by using a Philips Model 505/B microscope described elsewhere [9].

3. Results

3.1. Potential sweeping experiments in buffer with pH = 5.0

Voltammograms of tin in still 0.0244 M citric acid + 0.050 M sodium citrate solution, pH = 5.0, $I = 0.234$, run between $E_{s,c} = -1.90$ V and $E_{s,a} = 0.5$ V at $v = 0.1$ V s^{-1} are shown in Fig. 1a. Prior to the electrochemical experiments, any previously formed oxide was removed from the electrode surface by polarization at −1.9 V for 15 min. This electrode surface pretreatment ensured reproducibility and negligible differences between

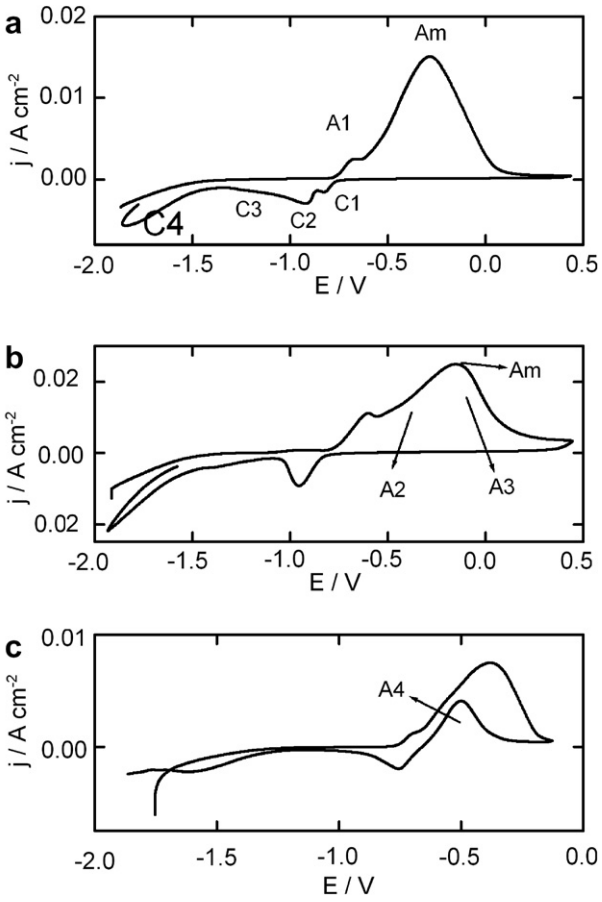

Fig. 1. Voltammograms of tin in still 0.0244 M citric acid + 0.050 M sodium citrate solution, pH = 5.0, $I = 0.234$, run between $E_{s,c} = -1.90$ V and $E_{s,a} = 0.5$ V (a) at $v = 0.1$ V s^{-1} and (b) at $v = 0.3$ V s^{-1}. (c) Voltammogram run between $E_{s,c} = -1.90$ V and $E_{s,a} = -0.13$ V at $v = 0.01$ V s^{-1}.

the response for the first and subsequent cycles. The positive-going potential scan exhibits two well defined anodic current peaks: a first peak (A1) at about −0.68 V was associated, in the literature, with the formation of Sn(II) species, and a main peak (Am) appearing at about −0.28 V, was interpreted as a result of the electroformation of Sn(IV)–containing species [11]. At the cathodic side of peak Am a broad shoulder, located between peaks A1 and Am, can be observed for certain working conditions, as discussed below. The anodic side of peak Am precedes a low intensity current plateau, which corresponds to the passivity region. The reverse scan exhibits at least four cathodic contributions (C1 through C4) located at ca. −0.82 V, −0.92 V, −1.19 V and −1.84 V, respectively.

The experiment shown in Fig. 1b was performed between the same switching potentials as in Fig. 1a but at $v = 0.3$ V s^{-1}, so that the shoulder located between peaks A1 and Am could be more clearly observed. This experimental feature together with the existence of multiple cathodic peaks in contrast to only two anodic contributions and an incoherent variation of peak current density j_{Am} with v, are all indications of the existence of an additional anodic contribution in the potential range limited

by peak potentials E_{A1} and E_{Am}. Consequently, a deconvolution procedure was used for resolving overlapped voltammetric peaks. In this way, peak Am can be separated into two distinctive anodic components that are strongly overlapped, namely A2 (corresponding to the above-mentioned shoulder) and A3 (located prior to the passive region).

Setting the anodic switching potential ($E_{s,a}$) at the descending side of peak Am ($E_{s,a} = -0.13$ V), prior to the passive region while sweeping the applied potential at low rates (typically <0.01 V s^{-1}), another anodic contribution (A4) can be detected during the reverse scan (Fig. 1c). This behaviour is qualitatively similar to that observed for tin electrodes in citric acid solution (pH = 1.8) [12] and corresponds to a reactivation process.

The asymmetry found in voltammetric peaks is mainly due to the influence of diffusion of the electroactive species from the bulk solution towards the electrode surface. Thus, with many surface processes (such as phase formation and removal or reaction of adsorbed species with Nernstian behaviour) no mass-transport effects are involved in the electrochemical reaction and voltammetric peaks are symmetric in shape [13,14]. In turn, the presence of symmetric peaks allows an optimized resolution of the voltammograms, from nonlinear regression analysis based on Gaussian functions. This inherently simpler approach was often followed for different electrochemical systems [15–17], and also for analogous systems [18], including the electrochemical behaviour of tin electrodes in borate buffer solutions [19,20].

For the present system only peaks A3 and C3 exhibit diffusional effects. Consequently, fitting of the current trace recorded during the anodic sweep (with null baseline correction), was performed from the potential for zero anodic current up to a potential value slightly exceeding the peak potential E_{Am}. Within this potential range the current response contains peaks A1 and A2 as well as that portion of peak A3 that excludes its possible asymmetric tailing. The analysis yielded peak locations and peak heights for all three anodic contributions. Additionally, charge densities for peaks A1 (q_{A1}) and A2 (q_{A2}) were calculated, while for peak A3 we report the charge density up to the maximum (q_{A3}). An analogous approach was adopted for the current trace recorded during the cathodic sweep, taking into account the same considerations for peak C3 as those already described for peak A3. Peak C4 strongly overlaps the hydrogen evolution region. In order to avoid inappropriate baseline corrections this contribution was not considered in the curve fitting procedure and it will be discussed below only on a qualitative basis. At this point it is probably worth mentioning that although peak C4 is present in some results published in the literature, its features have not been explored [5].

Fig. 2a shows the results of the fitting procedure applied to the current response recorded during the positive sweep (anodic) in terms of the single components and of the resulting calculated trace for the whole potential range.

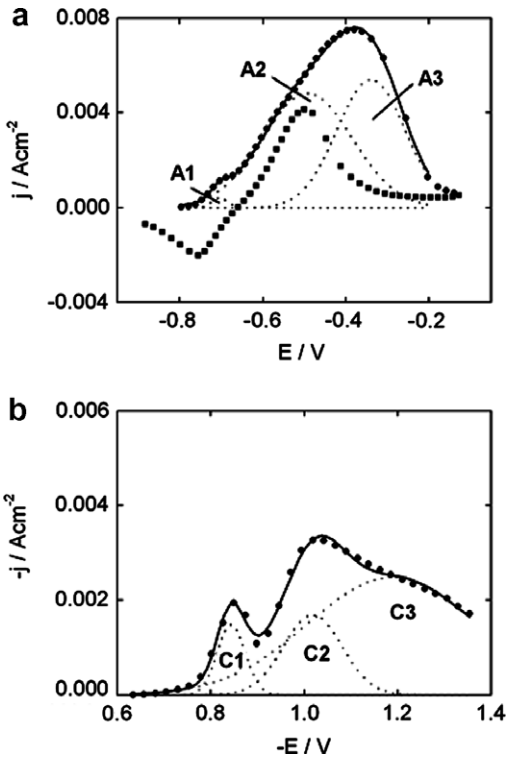

Fig. 2. (a) Voltammogram of tin in still 0.0244 M citric acid + 0.050 M sodium citrate solution, pH = 5.0, $I = 0.234$, at $v = 0.01$ V s^{-1}. (●) Experimental data recorded during the positive sweep in the potential region where the anodic contributions are present. Fit results: (—) calculated trace for the whole potential range and (---) calculated traces for the individual components. (■) Experimental data recorded during the reverse sweep. (b) Same conditions as (a) but with $v = 0.1$ V s^{-1}. (●) Experimental data recorded during the negative sweep in the potential region where the cathodic contributions are present.

These results demonstrate that a simple analysis of the experimental curve, i.e., without any deconvolution, can lead to erroneous interpretations, since the intensities of peaks A2 and A3 are comparable, at least under the working conditions for Fig. 2. For the sake of comparison experimental data corresponding to the reverse sweep (cathodic) are also included. These results also suggest that the reactivation process (A4) corresponds to the same process related to peak A2.

Fig. 2b shows one example of the results of the fitting procedure applied to the current response recorded during the reverse sweep. Single cathodic components are shown together with the resulting calculated current trace for the whole potential range.

3.1.1. Influence of the scan rate v

Dependencies of peak current density (j_{A1}), peak potential (E_{A1}) and charge density (q_{A1}) on v, for peak A1, are shown in Fig. 3. Both j_{A1} and E_{A1} vary linearly with the square root of the scan rate, while j_{A1} goes to zero as the scan rate goes to zero (Fig. 3a). These results can be interpreted in terms of a film formation process under ohmic resistance control [21,22], where the spread of a layer of

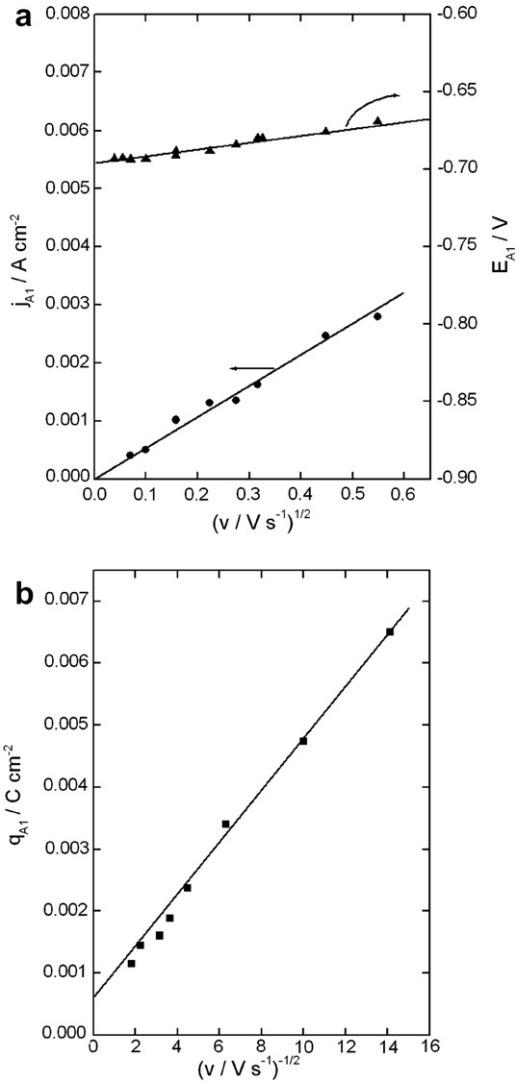

Fig. 3. Potential scan rate v dependences of (a) peak current density j_{A1} (●) and peak potential E_{A1} (▲) and (b) charge density q_{A1} (■), for peak A1. Data calculated from deconvoluted voltammograms of tin in still 0.0244 M citric acid + 0.050 M sodium citrate solution, pH = 5.0, $I = 0.234$.

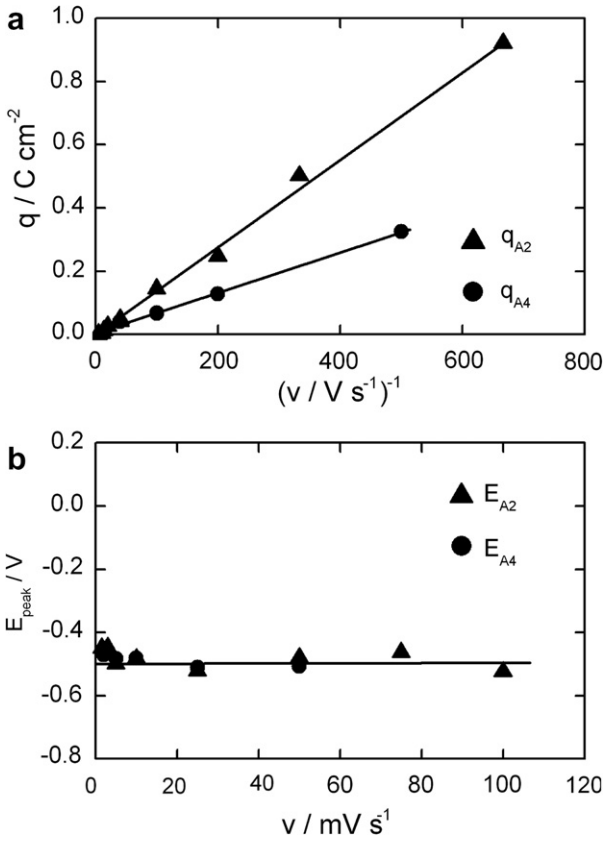

Fig. 4. (a) Dependences of charge densities for peaks A2 (▲) and A4 (●) on the potential scan rate v. Data calculated from deconvoluted voltammograms of tin in still 0.0244 M citric acid + 0.050 M sodium citrate solution, pH = 5.0, $I = 0.234$. (b) Dependences of peak potentials E_{A2} (▲) and E_{A4} (●) on the potential scan rate v. Data calculated from deconvoluted voltammograms as in (a) with $E_{s,a} = -0.13$ V.

reaction products on the electrode surface causes the change in ohmic resistance. The extrapolated value of q_{A1} for $v \to \infty$ is ca. 0.6 mC cm^{-2} (Fig. 3b). Taking into account a roughness factor of 2, as was previously reported [23], it is possible to estimate a value, 0.3 mC cm^{-2}, for the charge density related to the real electrode area. The charge for peak A1 corresponds to the formation of ca. one monolayer of Sn(II)-oxide assuming uniform coverage [24].

The effect of varying v on the charge densities for peaks A2 and A4 is shown in Fig. 4a. Thus, for decreasing sweep rates both q_{A2} and q_{A4} become larger according to a linear dependence on v^{-1}. The reactivation peak A4 probably occurs after a partial rupture of the film formed at more anodic potentials during the forward sweep. Consequently, during the reverse sweep when the potential reaches the initial part of peak A4 the number of available reactant sites for this electrooxidation process results smaller than that for the initial part of peak A2. In this way, q_{A4} results smaller than q_{A2} at all v, but with a common extrapolated value for $v \to \infty \approx 0.6$ mC cm^{-2} (after correction for the surface roughness). Moreover, peak potentials E_{A2} and E_{A4} exhibit similar values that are practically independent of v (Fig. 4b). These experimental findings support the assumption that both peaks are essentially due to the same electrochemical process.

Before discussing a particular reaction mechanism it is worth emphasizing that $q_{A2} > q_{A1}$ indicating that, where the inequality holds, the reaction or reactions related to peak A2 cannot be solely the oxidation of the surface species resulting from the reaction related to peak A1.

A comparison between experimental peak potentials extrapolated to $v \to 0$ and equilibrium potentials for possible reactions of tin electrodes can be made in order to select a descriptive reaction scheme [24]. From Fig. 3 results E_{A1} $(v \to 0) \approx -0.69$ V a value that roughly corresponds to the equilibrium potential $E_{Sn/SnO} = -0.64$ V at pH 5, assuming that the interfacial pH is larger than that in the bulk solution, due to the preceding hydrogen evolution reaction. This interpretation is supported by the fact that for rotated electrodes results E_{A1} $(v \to 0) \approx -0.64$ V in agreement with

the thermodynamic value. The experimental value E_{A2} ($v \to 0$) ≈ -0.50 V (Fig. 4b), compares well with the equilibrium potential $E_{Sn/Sn(OH)_4} = -0.54$ V at pH 5.

Dependencies of peak current density (j_{A3}), peak potential (E_{A3}) and charge density (q_{A3}) on v, for peak A3, are shown in Fig. 5. Both j_{A3} and E_{A3} vary linearly with the square root of the scan rate, while j_{A3} exhibits a small intercept on the j axis $\approx$0.003 A cm^{-2} (Fig. 5a). These results indicate that diffusional effects play an important role in the anodic reaction associated with peak A3 and leading to the passive state [5]. The extrapolated value of q_{A3} for $v \to \infty$ is ca. 5 mC cm^{-2} (Fig. 5b), or 2.5 mC cm^{-2} after correction for the surface roughness. Since this value corresponds to the charge density only up to the maximum, it is clear that the whole charge density for peak A3 largely exceeds that required for the oxidation of a monolayer of Sn(0) to Sn(IV) $\approx$0.74 mC cm^{-2}. Multilayer oxide formation and/or metal dissolution could account for this excess. It is of some interest to note that a dissolution-precipitation mechanism, as previously proposed in the literature [5], always produces a three-dimensional film and consequently monomolecular passivating layers can never result.

Dependencies of peak current density (j_{C1}), peak potential (E_{C1}) and charge density (q_{C1}) on v, for peak C1, are shown in Fig. 6. Both j_{C1} and E_{C1} vary linearly with the square root of the scan rate. While j_{C1} goes to zero as the scan rate goes to zero, E_{C1} shifts towards more negative potentials (Fig. 6a). The extrapolated value of q_{C1} for $v \to \infty$ is ca. 0.6 mC cm^{-2} (Fig. 6b) or 0.3 mC cm^{-2} after correction for the electrode surface roughness. Similarly to the analysis made for peak A1, these results can also be interpreted in terms of a film electroreduction process

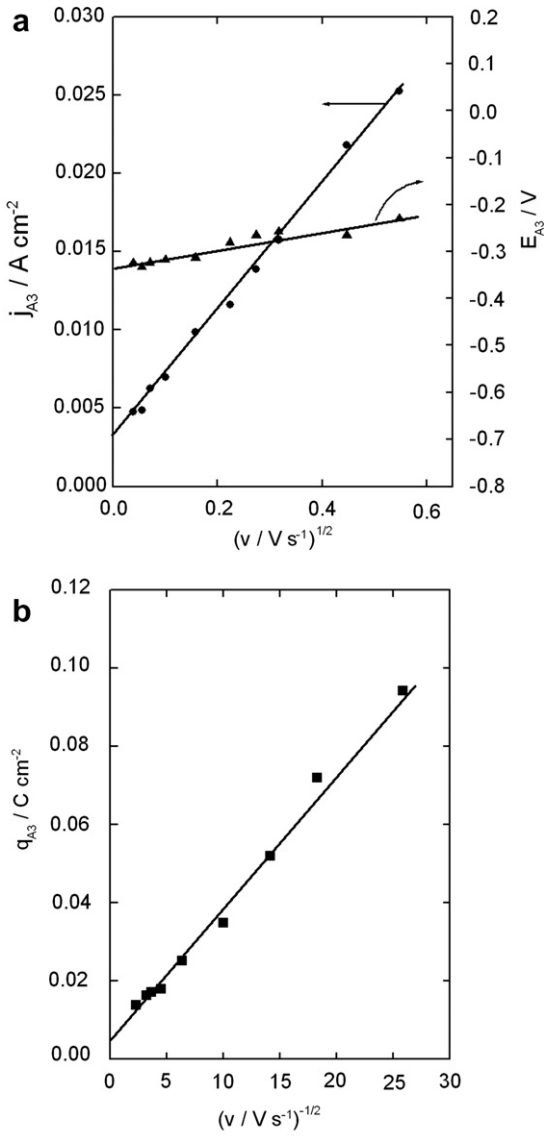

Fig. 5. Potential scan rate v dependences of (a) peak current density j_{A3} (●) and peak potential E_{A3} (▲) and (b) charge density q_{A3} (■), for peak A3. Data calculated from deconvoluted voltammograms of tin in still 0.0244 M citric acid + 0.050 M sodium citrate solution, pH = 5.0, I = 0.234.

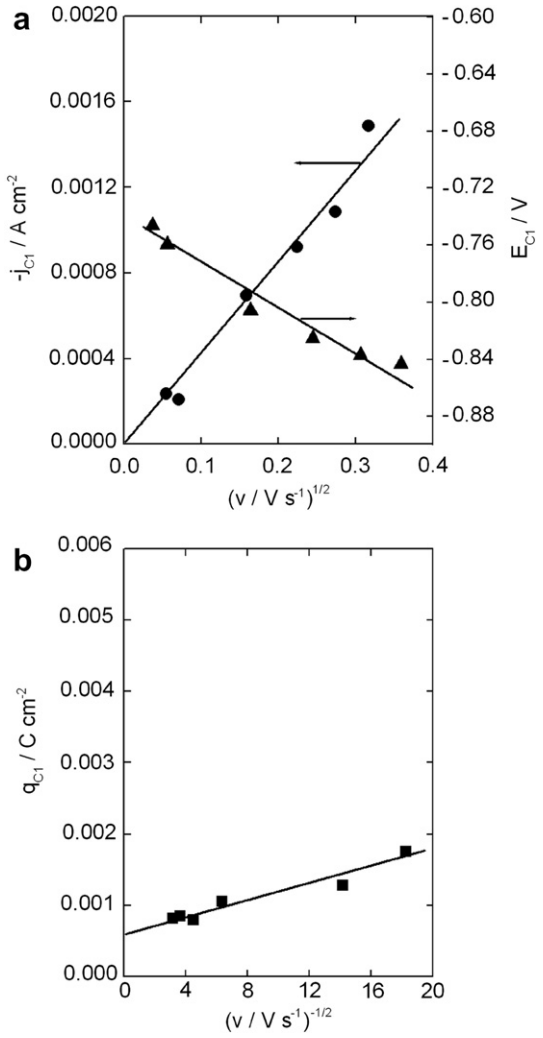

Fig. 6. Potential scan rate v dependences of (a) peak current density j_{C1} (●) and peak potential E_{C1} (▲) and (b) charge density q_{C1} (■), for peak C1. Data calculated from deconvoluted voltammograms of tin in still 0.0244 M citric acid + 0.050 M sodium citrate solution, pH = 5.0, I = 0.234.

under ohmic resistance control, where the extrapolated electroreduction charge for $v \to \infty$ corresponds to the reduction of about a monolayer of Sn(II) to Sn(0).

For peak C2 a plot of j_{C2} as a function of $v^{1/2}$ yields a straight line with a small intercept on the j axis, while E_{C2} shifts strongly to more negative potentials as v increases according to a linear E_{C2} vs. $v^{1/2}$ relationship (Fig. 7a). Thus, E_{C2} is shifted ca. 100 mV for each tenfold increase in v, a value larger than those measured for peaks A3 and C1. This behaviour indicates a greater degree of irreversibility of the electroreduction related to peak C2 and causes a large overlapping of peaks C2 and C3 for increasing v. This behaviour, in turn, determines that fitted data for $v > 0.05$ V s^{-1} are less reliable. The extrapolated value of q_{C2} for $v \to \infty$ is ca. 0.8 mC cm^{-2} (Fig. 7b) or 0.4 mC cm^{-2} after correction for the electrode surface roughness.

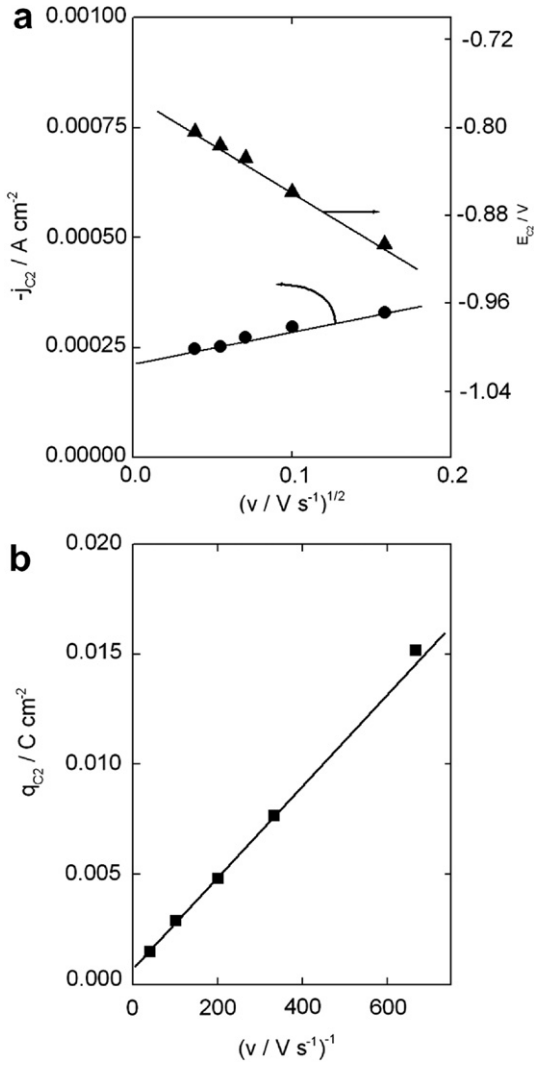

Fig. 7. Potential scan rate v dependences of (a) peak current density j_{C2} (●) and peak potential E_{C2} (▲) and (b) charge density q_{C2} (■), for peak C2. Data calculated from deconvoluted voltammograms of tin in still 0.0244 M citric acid + 0.050 M sodium citrate solution, pH = 5.0, $I = 0.234$.

Although peak C3 is poorly defined the observed sweep rate dependence is characterized by a slight shift of the peak potential E_{C3} towards more negative values while the charge density q_{C3} decreases as v decreases (data not shown). This behaviour can be understood in terms of the electroreduction of soluble tin species generated during the anodic sweep. Thus, lowering v causes that this species has more time to diffuse away from electrode surface and the amount of reactant available decreases.

Finally, peak C4 shifts to more negative potential values as v increases. It remains clearly observable at $v < 0.05$ V s^{-1}, although it always appears strongly superimposed on the hydrogen evolution reaction.

3.1.2. Influence of $E_{s,a}$ on the cathodic response

When $E_{s,a}$ is set within the potential range of peak A1 only peak C1 is present in the quantitatively analysed current trace recorded during the negative sweep. Fig. 8 shows charge densities for peaks C1, C2 and C3 calculated for different $E_{s,a}$ values. It can be seen that q_{C1} remains practically unaltered for all $E_{s,a}$. These results indicate that peak C1 is related to the electroreduction of a species generated in the potential range of peak A1 and that this species is not further oxidized at higher anodic potentials during the positive sweep. Charge density for peak C2 decreases as $E_{s,a}$ becomes more anodic in the passivity region. This could be the result of an initial passive layer that becomes increasingly transformed into a more stable compound that cannot be electroreduced in the potential range of peak C2. As for peak C3, it also exhibits decreasing charge density values for increasingly positive $E_{s,a}$ in the passivity region and in accordance with the time dependence of the process involved, as mentioned above in relation to the influence of v on peak C3 [25].

Peak C4 can still be detected even if $E_{s,a}$ is set within the potential range where the current goes to zero in the

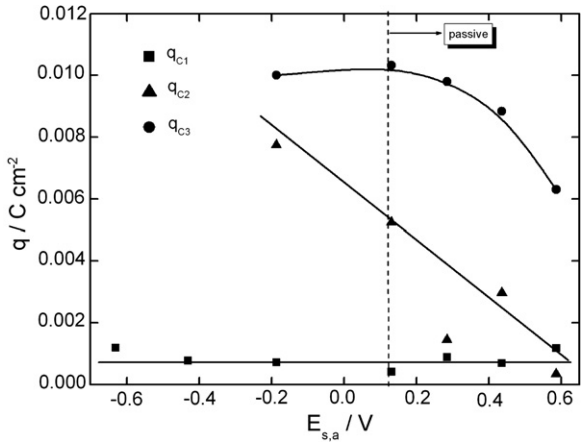

Fig. 8. Dependences of charge densities for peaks C1 (■), C2 (▲) and C3 (●) on the anodic switching potential ($E_{s,a}$). Data calculated from deconvoluted voltammograms of tin in still 0.0244 M citric acid + 0.050 M sodium citrate solution, pH = 5.0, $I = 0.234$ at $v = 0.1$ V s^{-1}. Potential region for the passive state is indicated.

forward scan. Consequently, the electroreduction process related to this peak cannot be directly linked to the anodic products that can be generated in the different anodic current contributions during the scan.

3.1.3. Influence of convection on the voltammetric response

Fig. 9 shows the influence of the rotation speed (ω) on the shape of voltammograms of a tin disk electrode in buffer with pH = 5.0 and $I = 0.234$. Most noticeable differences with the voltammograms measured in still solution are seen in the potential ranges for peaks A3 and C3. This indicates that the processes for peaks A1, A2 and C1 correspond mostly to solid-state transformations, i.e. no dissolved products or reactants are involved.

Charge densities determined for the anodic components and for C2 at different ω are shown in the insert of Fig. 9. Thus, q_{A1} and q_{A2} remain almost constant as ω increases, but q_{A3} decreases for increasing values of ω in the 0–1000 rpm range, becoming almost constant for higher rotation speeds up to 2500 rpm. It has previously been recognized that Sn^{4+} ions in citrate solutions can form many species that would lead to the formation of a passive film [5,26]. Thus, decreasing values of q_{A3} with ω could be understood in terms of the formation of soluble Sn(IV) – citrate complexes followed by hydrolysis to render a $Sn(OH)_4$ passive film (vide infra).

Under stirring conditions the stationary hydrodynamic boundary layer sets in and diffusion of protons away from the interface should operate under limiting rate conditions. This means that local acidification should be compensated by a mass-transport and consequently the anodic layer formation should require a relatively smaller charge as compared to the still electrode. Thus, higher rotation speeds enhance transport of protons away from the interface and film formation. This is the opposite case of increasing charge densities for enhanced transport of hydroxyl ions as reported for tin electrodes in NaOH solutions [27].

Reactivation peak A4 is not affected by electrode rotation, in agreement with the assumption that both peaks A2 and A4 are essentially due to the same electrochemical process.

As for peak C2, q_{C2} decreases for increasing values of ω in the 0–500 rpm range, becoming almost constant for higher rotation speeds up to 2500 rpm (insert of Fig. 9). This charge corresponds, to some degree, to the electroreduction of passive layers obtained at high anodic potentials.

Peak C3 was not present when the electrode was rotated rapidly; it presumably corresponds to reduction of dissolved anodic dissolution products.

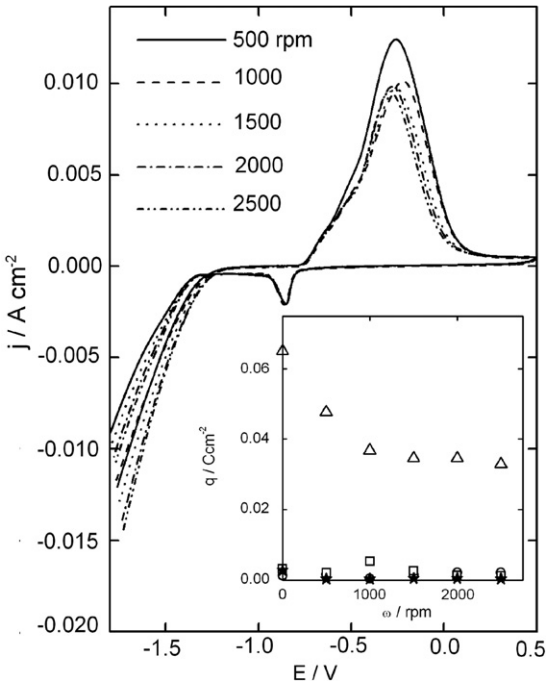

Fig. 9. Voltammograms of tin in 0.0244 M citric acid + 0.050 M sodium citrate solution, pH = 5.0, $I = 0.234$, at $v = 0.1$ V s^{-1} and at rotation speeds ω ranging from 500 to 2500 rpm. Insert: Charge densities for peaks A1 (○); A2 (□); A3 (△) and C2 (★) calculated from deconvoluted voltammograms at different ω as shown in Fig. 9.

3.2. Influence of the ionic strength I at constant pH

The effect of varying the ionic strength I at constant pH = 5 on the charge densities determined for each anodic peak is shown in Fig. 10a. As I is increased charge densities for peaks A1 and A2 remain practically unchanged. However, charge density for peak A3 increases with increasing values of I. Moreover, running the voltammograms for increasingly higher values of I results in a shift of E_{A3} to more positive values. In principle, reaction (3) could account for this behaviour. Thus, higher tin dissolution could result from accelerated rate for reaction (3) in the backward direction when the concentration of citrate ions in solution is increased.

Fig. 10b shows the influence of varying ionic strength on the cathodic voltammetric peaks. As the ionic strength is

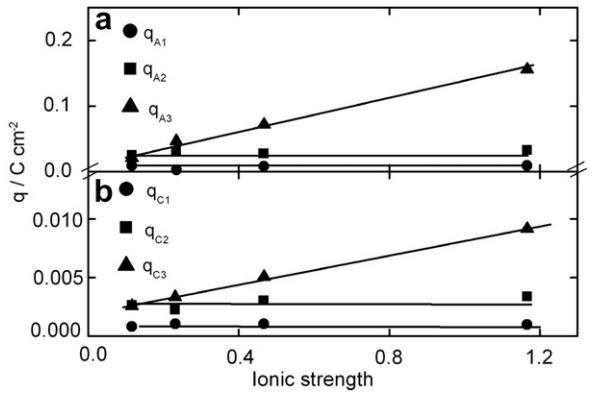

Fig. 10. (a) Charge densities for peaks A1 (●), A2 (■) and A3 (▲) calculated from deconvoluted voltammograms at different ionic strength I values. Data calculated from voltammograms of tin run in citrate buffer solution pH = 5.0 at $v = 0.025$ V s^{-1} and $E_{s,a} = 0.5$ V. (b) Same as (a) for peaks C1 (●), C2 (■) and C3 (▲).

increased charge densities for peaks C1 and C2 remain practically unchanged. On the other hand, charge density for peak C3 increases according to I. Again, this result supports the assumption that peak C3 could be related to the electroreduction of soluble Sn–citrate complexes.

3.3. Influence of solution pH at constant ionic strength

Voltammograms were recorded at constant ionic strength $I = 0.1167$ for increasingly higher values of pH in the range 3–6. Anodic peak potentials E_{A1}, E_{A2} and E_{A3} exhibit reasonably linear behaviour as a function of pH, with single slopes close to 60 mV/unit pH for the whole pH range (Fig. 11a) that could be explained on the basis of the equilibrium reactions of oxide and hydroxide formation. Values as high as 200 mV/unit pH were reported in the literature for the slope dE_{Am}/dpH in the pH range 3–5 and 110 mV/unit pH in the pH range 5–6. It becomes clear, after examining Fig. 2a that a large difference can exist between E_{Am} and E_{A2}. This situation again demonstrates the need to deconvolute overlapped contributions before discussing the particular reaction mechanisms. An analogous behaviour was measured for cathodic peak potentials E_{C1}, E_{C2} and E_{C3} (Fig. 11b).

Charge densities determined for the anodic components in the studied pH range are shown in Fig. 12a. In particular, q_{A3} exhibits, by far the most marked variation with the buffer's pH value. It attains a maximum value in the buffer with pH 4. This result indicates that tin exhibits a significant anodic dissolution at this pH in agreement with previously published results [5,28].

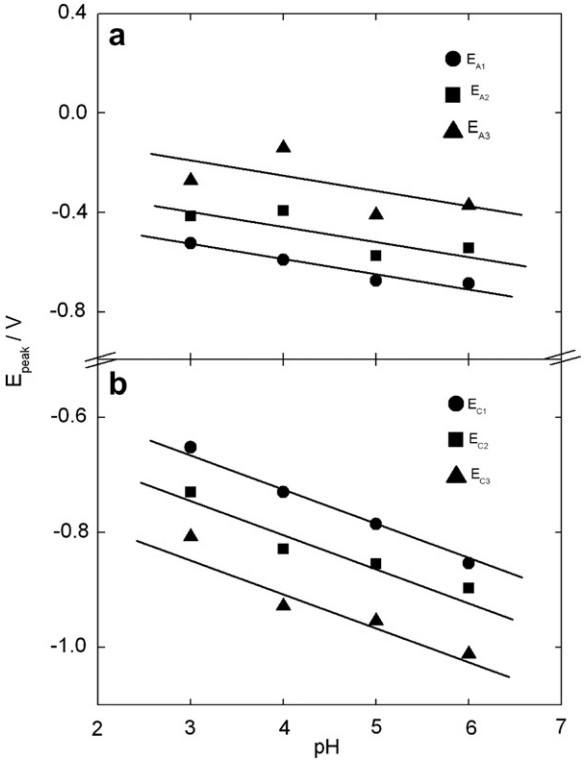

Fig. 11. Dependences of peak potentials on the pH values of the buffers with $I = 0.1167$. Data from voltammograms run at $v = 0.025$ V s^{-1}, (a) for anodic peaks A1 (●), A2 (■) and A3 (▲) and (b) for cathodic peaks C1(●), C2 (■) and C3 (▲).

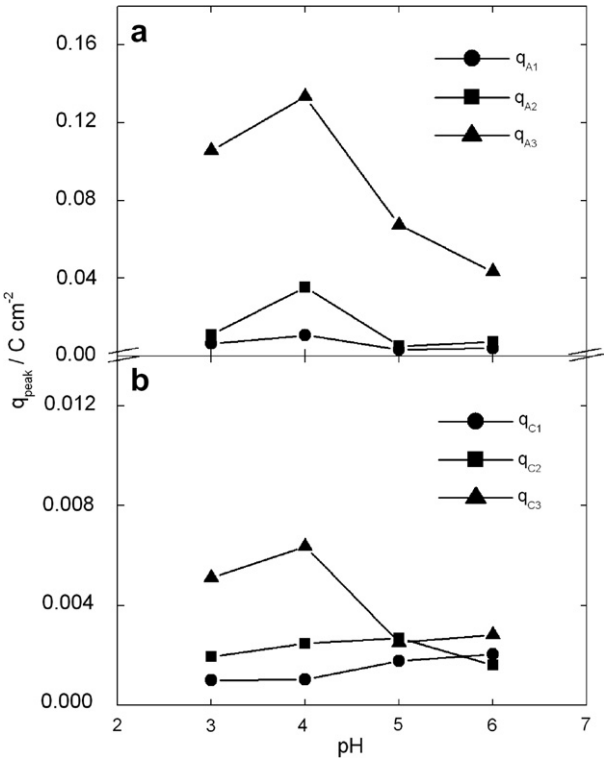

Fig. 12. Dependences of charge densities on the pH values of the buffers with $I = 0.1167$. Data from voltammograms run at $v = 0.025$ V s^{-1}, (a) for anodic peaks A1 (●), A2 (■) and A3 (▲) and (b) for cathodic peaks C1 (●), C2 (■) and C3 (▲).

As shown in Fig. 12b q_{C3} exhibits the same behaviour as q_{A3} when the buffer pH is varied over the 3–6 pH range. This result reinforces the view that peak C3 could be related to the electroreduction of soluble tin species generated in the electrooxidation process related to peak A3.

3.4. SEM observations

SEM micrographs were obtained for tin surfaces oxidized at different applied potentials. A linear potential sweep at $v = 0.010$ V s^{-1} was applied up to $E_{s,a}$ set in the potential range of peaks A_1, A_2, A_3 and A_4, and finally a potential holding was applied at the selected $E_{s,a}$ value for 10 min.

Fig. 13a shows a SEM image of the electrode surface after setting $E_{s,a} = E_{A1}$. A continuous ultra-thin film covers the surface. Low film thickness renders a featureless morphology, while lines arising from the mechanical polishing can be clearly observed. This surface film could be related to the Sn(0) → Sn(II) reaction. At this potential dark areas corresponding to islands of a denser film can also be

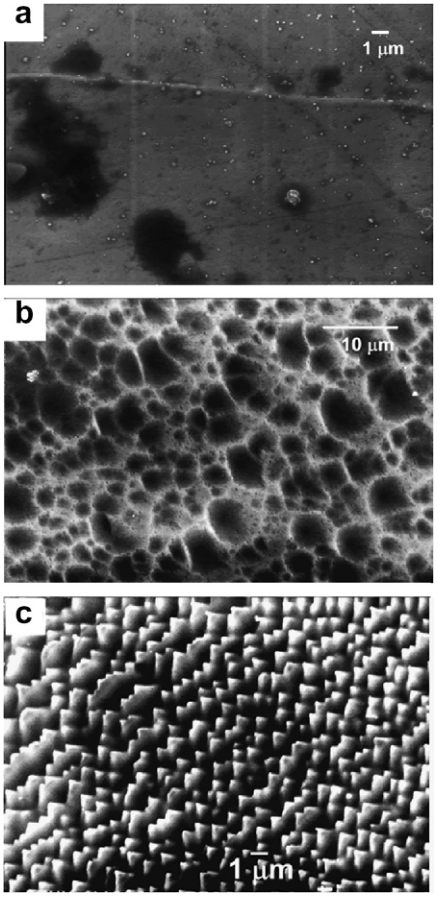

Fig. 13. (a) SEM image of the tin surface after the application of a linear potential sweep at $v = 0.010\ \mathrm{V\ s^{-1}}$ up to $E_{s,a} = E_{A1}$ and a potential holding at $E_{s,a}$ for 10 min; (b) after the application of a linear potential sweep at $v = 0.010\ \mathrm{V\ s^{-1}}$ up to $E_{s,a} = E_{A2}$ and a potential holding at $E_{s,a}$ for 10 min and (c) as in (b) showing a different zone (magnification × 4000).

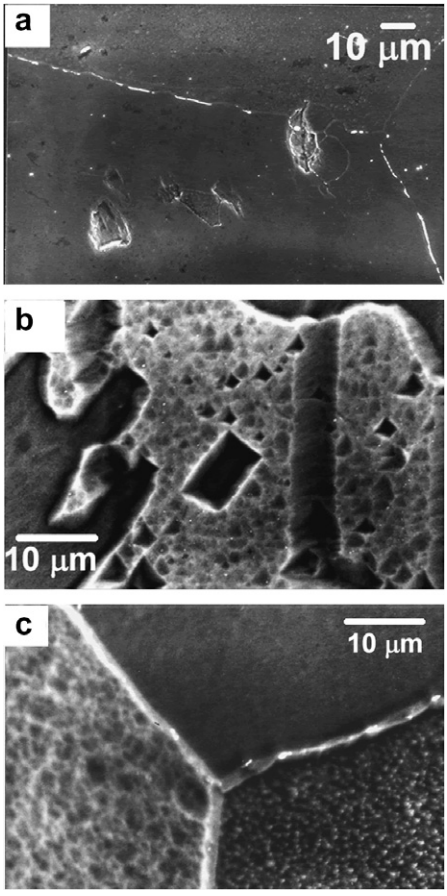

Fig. 14. (a) SEM image of the tin surface after the application of a linear potential sweep at $v = 0.010\ \mathrm{V\ s^{-1}}$ up to $E_{s,a} = E_{A3}$ and a potential holding at $E_{s,a}$ for 10 min; (b) after the application of an anodic potential sweep up to −0.1 V immediately followed by a cathodic sweep entering the potential region corresponding to the reactivation process and holding the potential at E_{A4} (magnification × 2000) and (c) as in (b) showing a different zone.

observed suggesting the occurrence of a second surface process probably related to the initial portion of peak A2. Voltammetric analysis indicates that the end of the Sn(0) → Sn(II) reaction overlaps the beginning of the Sn(0) → Sn(IV) reaction.

SEM examination of the electrode surface after the application of a linear potential sweep with $E_{s,a} = E_{A2}$ reveals the existence of a film layer characterized by zones exhibiting at least two different morphologies. Fig. 13b shows a surface film with a spongy porous structure. On the other hand a fully faceted and highly oriented growth was observed in a different region. Prismatic clusters with dimensions even above a micrometer are shown in Fig. 13c.

SEM images recorded after holding the potential at E_{A3} (Fig. 14a) show the tin surface coated by a thick compact oxide with occasional appearing of islands of voluminous anodic products. This film corresponds to the truly passivating layer ascribed to Sn(IV)-species.

SEM images in Fig. 14b and c correspond to electrodes after the application of an anodic potential sweep up to −0.1 V immediately followed by a cathodic sweep entering the potential region corresponding to the reactivation process and holding the potential at E_{A4}. The SEM micrograph in Fig. 14b shows the presence of a thick epitaxial oxide film, probably formed during the sweep in the potential region of peak A3, which covers only partially the electrode surface. Preferential dissolution at grain boundaries can also be observed [29]. The morphology of the oxide grown underneath exhibits different features according to the proper crystallographic orientation of each grain (Fig. 14c). These different morphologies can be unambiguously correlated with those observed after holding the potential at E_{A2} and described for Fig. 13b and c. These results confirm the assumption that both peaks A2 and A4 are essentially due to the same electrochemical process. A close inspection reveals that the dissolution process occurs more intensely along grain boundaries.

4. Discussion

The simplest mechanism, which accounts for all the experimental results presented in this work and those lead-

ing to the model of the passive film proposed by Keller et al. [7] can be put forward as follows.

Initially a thin film of SnO is formed at potentials related to peak A1 following reaction (1). This film is not further oxidized at higher anodic potentials

$$Sn + H_2O \leftrightarrows SnO + 2H^+ + 2e^- \quad (1)$$

Since long ago the majority of workers in this field have subscribed to the opinion that the prepassive film consists of SnO [27]. Additionally, direct oxidation of tin to a thin layer of Sn(IV) hydroxide takes place according to reaction (2) that can be associated with peak A2

$$Sn + 4H_2O \leftrightarrows Sn(OH)_4 + 4\ H^+ + 4\ e^- \quad (2)$$

The reaction associated with peak A3 involves the formation of soluble Sn(IV) ions that in citrate solutions could form a complexed species. Secondary passivation follows and is due to the formation of a multilayer of $Sn(OH)_4$ according to reaction (3) that could be tentatively expressed as

$$Sn(Hcit)_2 + 4\ H_2O \leftrightarrows Sn(OH)_4 + 4\ H^+ + 2\ Hcit^{2-} \quad (3)$$

There is general agreement that since $Sn(OH)_4$ is extremely insoluble; it precipitates on the electrode surface and in the pores of the existing layer of surface products giving rise to a truly passivating film. It is also generally accepted that the $Sn(OH)_4$ film evolves to a more thermodynamically stable SnO_2 film with time and increasing anodic polarization.

Under working conditions that enable peak A4 to be detected rupture of the passive film takes place and the same anodic process as that related to peak A2 occurs during the negative sweep.

Probably due to a different behaviour between freshly polished electrodes and reformed electrodes [8], the preceding interpretation does not fully agree with three propositions about the mechanistic pathway previously proposed for the potentiodynamic oxidation of tin in citrate buffers pH 3–6. These propositions are [5]: (i) the existence of different descriptive mechanisms according to the pH of the buffer; (ii) a stepwise oxidation $Sn(0) \rightarrow Sn(II) \rightarrow Sn(IV)$ and finally, (iii) the generation of soluble Sn(II), as the main dissolved species, during the forward scan. On the other hand, direct oxidation of the tin surface to Sn(IV) species (repeatedly postulated in the literature [9,27,30,31]), either as soluble ions or as a hydroxide layer, seems to be more likely to occur under our experimental conditions during the sweep in the potential ranges of peaks A2 and A3.

During the negative sweep the Sn(II)-oxide film is first electroreduced following a reaction that can be associated with peak C1. The process related to peak C2 corresponds to the electroreduction of the initially formed passive layer described in the literature as an amorphous $Sn(OH)_4$ film. This species evolves after dehydration to a more stable compound that becomes increasingly more difficult to be electroreduced. The most stable species was reported to be the hydrated oxide $SnO_2 \cdot H_2O$ and its formation is a function of both increasing positive potentials and time [24]. Dissolved anodic dissolution products generated during the positive sweep (peak A3) can be reduced during the negative sweep according to a reaction under mass-transport control and related to peak C3. Similarly, three cathodic peaks were previously observed in the potentiodynamic response of tin electrodes in Na_2SO_4 solutions and were ascribed to the reduction of dissolved anodic species of tin, SnO_2 and SnO respectively [32].

5. Conclusions

Voltammetric experiments were performed with tin electrodes in citrate buffer solutions at pH ranging from 3 to 6. SEM was used to examine the morphology of the anodic surface products generated in different potential regions during the scan.

By choosing the working conditions carefully it was possible to find the origin of some inconsistency observed in previous publications [5,6]. Our conditions involve the following actions: correcting the voltammograms for ohmic drop, separating the effects of different variables (pH and ionic strength) and finally, working over wider ranges of v and ω. Moreover, since all voltammograms have shown the superposition of some processes, a numerical deconvolution approach was used to resolve into single components the complex electrochemical behaviour observed.

Some evidence indicates that the electrooxidation pathway can be described by a single mechanism irrespective of the buffer pH. Direct oxidation of the tin surface to Sn(IV) species leads to secondary passivity, rather than a sequential oxidation $Sn(0) \rightarrow Sn(II) \rightarrow Sn(IV)$.

Acknowledgements

Dr. Gervasi gratefully acknowledges the Comisión de Investigaciones Científicas y Técnicas Buenos Aires (CICBA) for his position as a member of the Carrera del Investigador Científico. This work was financially supported by Consejo Nacional de Investigaciones Científicas y Técnicas, Consejo de Investigaciones de la Universidad Nacional de Tucumán and CICBA. The authors acknowledge the assistance of A. Andrada Barone with the SEM micrographs.

References

[1] S.S. Abd El-Rehim, S.M. Sayyah, M.M. El Deeb, Mater. Chem. Phys. 80 (2003) 696.
[2] S.S. Abd El-Rehim, H.H. Hassan, N.F. Mohamed, Corros. Sci. 46 (2004) 1071.
[3] C.M.V.B. Almeida, B.F. Giannetti, Mater. Chem. Phys. 69 (2001) 261.
[4] T.D. Burleigh, H. Gerischer, J. Electrochem. Soc. 135 (1988) 2938.
[5] M. Šeruga, M. Metikoš-Huković, J. Electroanal. Chem. 334 (1992) 223.
[6] M. Šeruga, M. Metikoš-Huković, T. Valla, M. Milun, H. Hoffschultz, K. Wandelt, J. Electroanal. Chem. 407 (1996) 83.

[7] P. Keller, H-H. Strehblow, Z. Phys. Chem. 219 (2005) 1481.
[8] P. Keller, Ph.D. Thesis, Heinrich-Heine University, Düsseldorf, Germany 2006. Available from: <http://diss.ub.uni-duesseldorf.de/home/etexte/diss/diss_files/1305.pdf>.
[9] P.E. Alvarez, S.B. Ribotta, M.E. Folquer, C.A. Gervasi, J.R. Vilche, Corros. Sci. 44 (2002) 49.
[10] C.A. Gervasi, P.E. Alvarez, Corros. Sci. 47 (2005) 69.
[11] M. Metikoš-Huković, S. Omanović, A. Jukić, Electrochim. Acta 45 (1999) 977.
[12] B.F. Giannetti, P.T.A. Sumodjo, T. Rabockai, J. Appl. Electrochem. 20 (1990) 672.
[13] S. Menolasina, in: Fundamentos y aplicaciones de Electroquímica, Mérida 2004, Universidad de Los Andes, Consejo de Publicaciones, pp. 121–127 (in Spanish).
[14] Southampton Electrochemistry Group in Instrumental Methods in Electrochemistry, New York 1985, Ellis Horwood Ltd., pp. 206–209.
[15] A. Martins, V. Ferreira, A. Queirós, I. Aroso, F. Silva, J. Feliu, Electrochem. Commun. 5 (2003) 741–746.
[16] A.E. Bolzán, R.C.V. Piatti, A.J. Arvia, J. Electroanal. Chem. 552 (2003) 19.
[17] J.P.F. Matos, L. Proença, M.I.S. Lopes, I.T.E. Fonseca, J. Electroanal. Chem. 571 (2004) 111.
[18] D. Gallant, M. Pézolet, A. Jacques, S. Simard, Corros. Sci. 48 (2006) 2547.
[19] R. Díaz, I. Díez-Pérez, P. Gorostiza, F. Sanz, J.R. Morante, J. Braz. Chem. Soc. 14 (2003) 523.
[20] R. Díaz Delgado, Ph.D. thesis, University of Barcelona, Spain, 2002. Available from: <www.tdx.cesca.es/TDX-1018102-110211/>.
[21] A.J. Calandra, N.R. de Tacconi, R. Pereiro, A.J. Arvia, Electrochim. Acta 19 (1974) 901.
[22] W.J. Müller, Trans. Faraday Soc. 27 (1931) 737.
[23] C.A. Gervasi, M.E. Folquer, A.E. Vallejo, P.E. Alvarez, Electrochim. Acta 50 (2005) 1113.
[24] S.D. Kapusta, N. Hackerman, Electrochim. Acta 25 (1980) 1625.
[25] P.E. Alvarez, C.A. Gervasi, Corros. Sci. 46 (2004) 91.
[26] A. Szorcsik, L. Nagy, B. Gyurcsik, Gy. Vankó, R. Krämer, A. Vértes, T. Yamaguchi, K. Yoshida, J. Radioanal. Nucl. Chem. 260 (2004) 459.
[27] B.N. Stirrup, N.A. Hampson, J. Electroanal. Chem. 67 (1976) 45.
[28] V.K. Gouda, E.N. Rizkalla, S. Abd-El-Wahab, E.M. Ibrahim, Corros. Sci. 21 (1981) 1.
[29] B.F. Giannetti, P.T.A. Sumodjo, T. Rabockai, A.M. Souza, J. Barboza, Electrochim. Acta 37 (1992) 143.
[30] D. Eurof Davies, S.N. Shah, Electrochim. Acta 8 (1963) 703.
[31] M. Drogowska, H. Ménard, L. Brossard, J. Appl. Electrochem. 21 (1991) 84.
[32] S.S. Abd El-Rehim, F. Taha, M.B. Saleh, S.A. Mohamed, Corros. Sci. 33 (1992) 1789.